ELSEVIER

Thermochimica Acta 253 (1995) 253–264

thermochimica acta

Pyrolytic process of La(III)–Cr(VI) precursor for the perovskite type lanthanum chromium oxide ☆

Atsushi Furusaki *, Hidetaka Konno, Ryusaburo Furuichi

Research Group of Materials Chemistry, Graduate School of Engineering, Hokkaido University, Kita-ku, Sapporo 060, Japan

Received 11 July 1994; accepted 11 July 1994

Abstract

The kinetics of the conversion of monazite type $LaCrO_4$ to perovskite type $LaCrO_3$ have been investigated by isothermal TG. The kinetics are dependent on the partial oxygen pressure and the conversion reaction is clearly suppressed with increase of pressure. The appropriate model functions for the kinetics are determined based on the Avrami–Erofe'ev equation. In nitrogen, the rate determining step is a three-dimensional phase-boundary reaction ($R_3(\alpha)$ function) and the activation energy E_a is estimated to be about 198 kJ mol^{-1}. In oxygen, three-dimensional diffusion of oxygen through the $LaCrO_3$ layer is the rate determining step ($D_3(\alpha)$ Jander function) with E_a of about 506 kJ mol^{-1}. For the latter case deoxygenation might proceed via an intermediate state in which oxygen adsorbs on the $LaCrO_3$ surface.

Keywords: Lanthanum chromium oxide; Mixed oxide; Model; Monazite; Perovskite; Pyrolysis; TG

1. Introduction

Synthesis of perovskite type $LaCrO_3$ has been investigated for the application to separator or interconnector materials in solid oxide fuel cells [1–6]. Mostly the starting materials were La(III)–Cr(III) compounds, although a few investigators

* Corresponding author.

☆ Presented at the International and III Sino–Japanese Symposium on Thermal Measurements, Xi'an, 4–6 June 1994.

SSDI 0040-6031(94)02024-8

used the La(III)–Cr(VI) system [7,8]. When the precursor prepared from La(III)–Cr(VI) solutions was pyrolyzed under appropriate conditions, a single phase of monazite type $LaCrO_4$ containing Cr(V) was formed as an intermediate. By further pyrolysis it decomposed to $LaCrO_3$ and the pyrolytic reaction was affected by the partial oxygen pressure in the atmosphere [8]. Although the preparation and characterization of $LaCrO_4$ have been reported [9–12], the decomposition mechanism to $LaCrO_3$ is not reported.

In the present work, the kinetics of the reaction

$$LaCrO_4(\text{monoclinic}) \rightarrow LaCrO_3(\text{orthorhombic}) + 0.5O_2 \quad (1)$$

have been studied by isothermal TG.

2. Experimental

2.1. Preparation of $LaCrO_4$

The compound $LaCrO_4$ was formed by pyrolysis of a La(III)–Cr(VI) precursor at 600°C in air for 1 h; the precursor was prepared by vacuum condensation of an equimolar solution of $La(CH_3COO)_3 \cdot 1.5H_2O$ (guaranteed reagent, Kanto Chemical Co., Ltd.) and CrO_3 (guaranteed reagent, Kanto Chemical Co., Ltd.) at 70°C with a rotary evaporator (RE-111, Shibata Co., Ltd.), followed by heat treatment at 400°C in air. Details have been reported elsewhere [8]. The $LaCrO_4$ formed was confirmed to be a single phase by X-ray diffraction (XRD) (ME-412C, Toshiba Co., Ltd.) using Cu Kα radiation and by chemical analysis after dissolving in 0.1 M HNO_3 (complexometric titration for lanthanum) or in 2 M H_2SO_4 (modified diphenylcarbazide method [13] for chromium).

2.2. Isothermal TG

The isothermal TG measurements were carried out with TG–DTA 2000 (Mac Science Co., Ltd.). A typical temperature program and TG curve are shown in Fig. 1. About 3 mg of the sample was heated in a stream of N_2, air or O_2 (100 cm^3 min^{-1}) with an infrared image furnace at 30 K s^{-1} from room temperature to the pre-heating temperature, T_{pre}, which was 130–160 K below the lowest reaction temperature, and held for 20 min. Then the sample was heated further at the same heating rate to the programmed reaction temperature, T_{reac}, and the TG measurement was performed isothermally. Reaction time t_{reac} counting commenced when the sample temperature reached T_{reac}. The reaction period (holding time) was 60 min. The fraction reacted α was calculated from measured mass loss Δm.

2.3. Morphologies

Morphologies of $LaCrO_4$ and $LaCrO_3$ powder were observed by scanning electron microscopy (SEM) (S-4000, Hitachi Co., Ltd.; 15 keV). The $LaCrO_4$

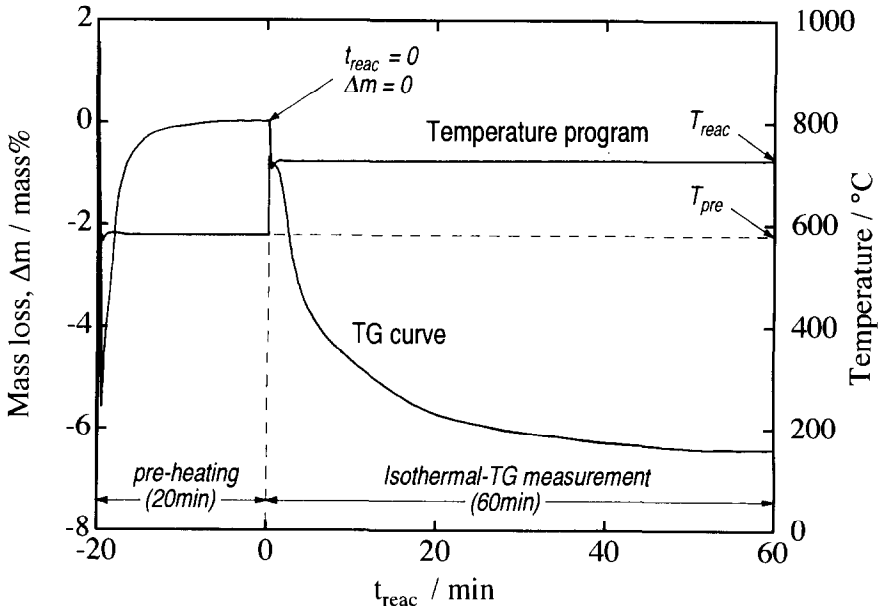

Fig. 1. Typical temperature program and measured TG curve: sample mass, 2.81 mg; heating rate, 30 K s^{-1}; T_{pre}, 580°C; T_{reac}, 725°C; atmosphere, O_2 (100 cm^3 min^{-1}).

sample was as-prepared, and $LaCrO_3$ was formed by the pyrolysis of this $LaCrO_4$ at 650°C for 1 h in a stream of N_2. Powder samples were dispersed ultrasonically in ethanol and mounted on glass plates. After evaporation of ethanol, they were coated with gold by d.c. sputtering (SPM-112, Neva Co., Ltd.; Ar 20 Pa, 1.2 kV, 10 mA, 1 min).

3. Results and discussion

An example of a measured TG curve is shown in Fig. 1. The rapid decrease followed by gradual increase of sample mass observed in the initial period of pre-heating arises from buoyancy which is unavoidable with the instrument used: the same behavior was observed during the blank tests using an Al_2O_3 sample. In order to avoid the heat-transfer effects on the sample powder, the sample mass was taken to be small (ca. 3 mg). Reproducibility of the measured Δm was in the approximate range $\pm 5\%$.

The decomposition reaction of $LaCrO_4$ is considered to be composed of the following four elementary reactions: (i) nucleation and growth of $LaCrO_3$; (ii) a phase-boundary reaction between $LaCrO_4$ and $LaCrO_3$; (iii) diffusion of oxygen species through the $LaCrO_3$ layer; and (iv) evolution of O_2 gas. Analysis of the kinetic data was carried out using a method which was proposed by Hancock and

Table 1
Values of m for solid state reaction rate equations [15]

Function	Equation	m [a]
$D_1(\alpha)$	$\alpha^2 = kt$	0.62
$D_2(\alpha)$	$(1-\alpha)\ln(1-\alpha)+\alpha = kt$	0.57
$D_3(\alpha)$	$[1-(1-\alpha)^{1/3}]^2 = kt$	0.54
$D_4(\alpha)$	$(1-2/3\alpha)-(1-\alpha)^{2/3} = kt$	0.57
$F_1(\alpha)$	$-\ln(1-\alpha) = kt$	1.00
$R_2(\alpha)$	$1-(1-\alpha)^{1/2} = kt$	1.11
$R_3(\alpha)$	$1-(1-\alpha)^{1/3} = kt$	1.07
Zero order	$\alpha = kt$	1.24
$A_2(\alpha)$	$[-\ln(1-\alpha)]^{1/2} = kt$	2.00
$A_3(\alpha)$	$[-\ln(1-\alpha)]^{1/3} = kt$	3.00

[a] $\ln[-\ln(1-\alpha)] = \ln B + m \ln t$.

Sharp [14] based on the Avrami–Erofe'ev [15,16] (or Johnson–Mehl [17]) equation

$$\alpha = 1 - \exp(-Bt^m) \tag{2a}$$

or

$$\ln[-\ln(1-\alpha)] = \ln B + m \ln t \tag{2b}$$

where α is a fraction reacted, B is a constant which depends on the nucleation frequency and linear rate of grain growth, and m is a constant that can vary according to the geometry of the system. In this method there are ten $f(\alpha)$ functions which are classified into three groups as shown in Table 1: (1) diffusion controlled models ($D_1(\alpha)$ to $D_4(\alpha)$), (2) nucleation growth controlled models ($F_1(\alpha)$, $A_2(\alpha)$ and $A_3(\alpha)$), (3) phase-boundary controlled models ($R_2(\alpha)$ and $R_3(\alpha)$). These groups are identified by the value of m as can be seen in Table 1. Fig. 2(a)–(c) shows the plots

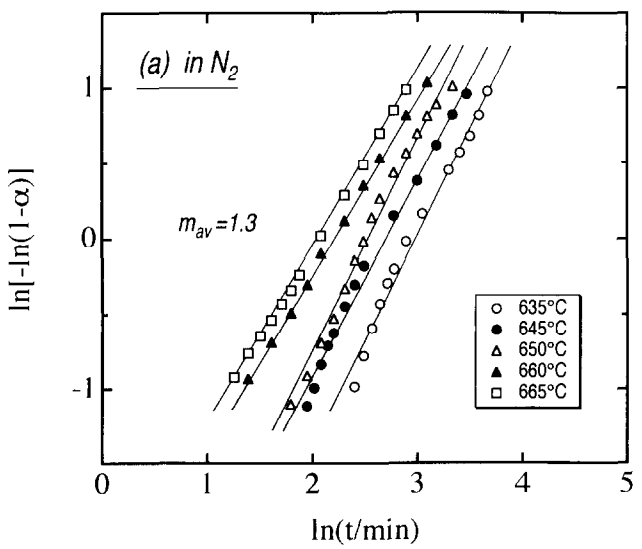

(a)

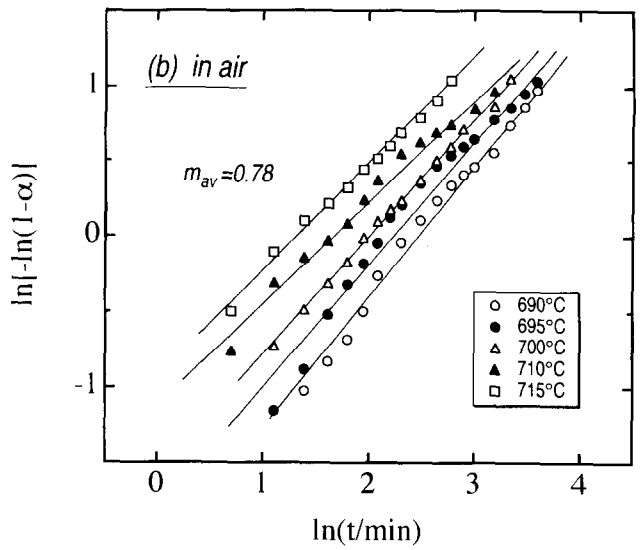

(b)

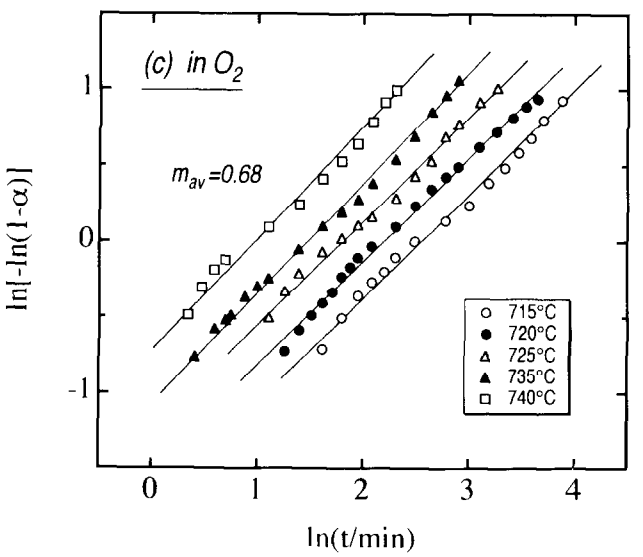

(c)

Fig. 2. Plots of $\ln[-\ln(1-\alpha)]$ against $\ln t$ in the range $0.25 < \alpha < 0.95$ at different temperatures: (a) N_2; (b) air; (c) O_2 (100 cm^3 min^{-1}).

of $\ln[-\ln(1-\alpha)]$ against $\ln t$ in the range of $0.25 < \alpha < 0.95$. The plots are almost linear with average m values of about 1.3 for N_2, 0.78 for air, and 0.68 for O_2. These m values suggest that the kinetics in N_2 are explained by the nucleation growth controlled model ($F_1(\alpha)$), phase-boundary controlled models ($R_2(\alpha)$ and $R_3(\alpha)$), or the zero order model, and in O_2 by diffusion controlled models ($D_1(\alpha)$–$D_4(\alpha)$). There was no single model applicable to air, so that the decomposition in air may proceed by mixed models.

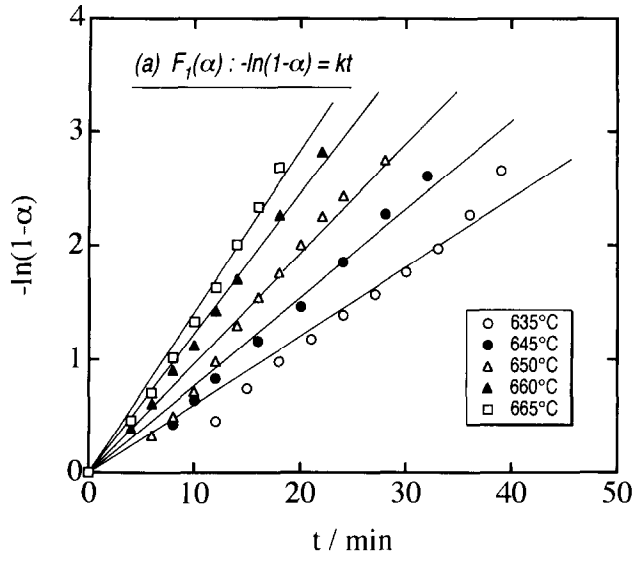

(a)

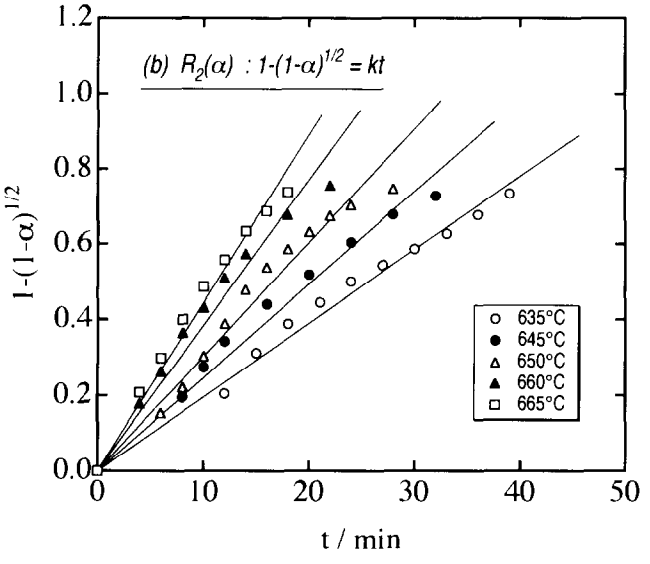

(b)

Fig. 3(a,b).

In order to find the most appropriate kinetic function, linear fitting of the data to each function was attempted. As found from Fig. 3(a)–(d), the data in N_2 fitted to $F_1(\alpha)$, $R_2(\alpha)$ and $R_3(\alpha)$ functions fairly well. In the range of $0.25 < \alpha < 0.95$, however, the three-dimensional phase-boundary controlled model $R_3(\alpha)$ showed better linearity than $F_1(\alpha)$ and $R_2(\alpha)$. This suggests that the shell of products covers the reactant particles and the phase-boundary reaction is the rate determining step,

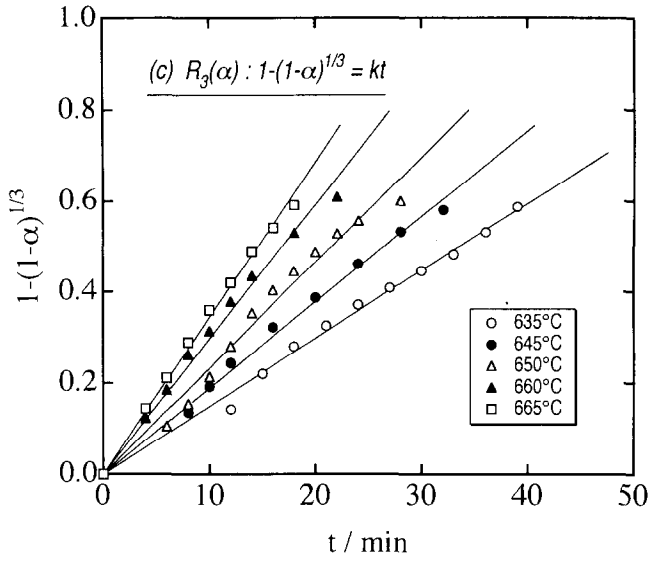

(c)

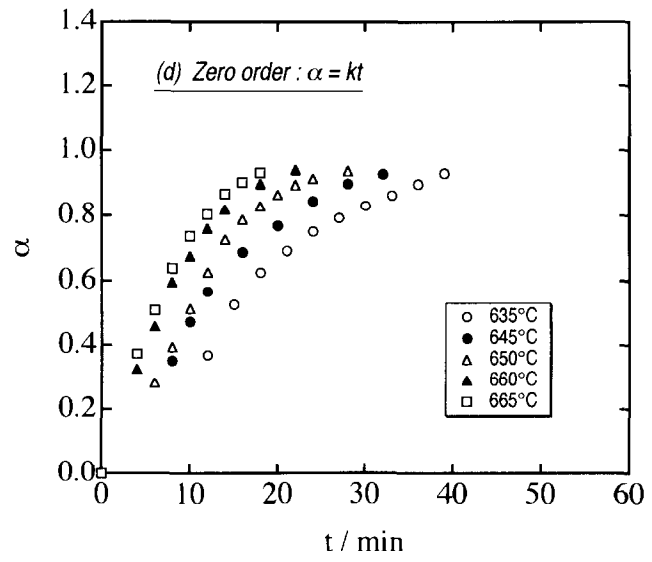

(d)

Fig. 3. Linear fittings of model functions for a N_2 atmosphere for data in Fig. 2(a): (a) $F_1(\alpha)$; (b) $R_2(\alpha)$; (c) $R_3(\alpha)$; (d) zero order.

where boundary area decreases with the progress of reaction. The data in O_2 showed the best fitting to the $D_3(\alpha)$ Jander function as can be seen in Fig. 4(c), which implies that the spherical particles are covered with a dense product layer and diffusion of a species through the layer is the rate determining step. In the present case, the diffusion species is presumed to be oxygen; accordingly it is expected that

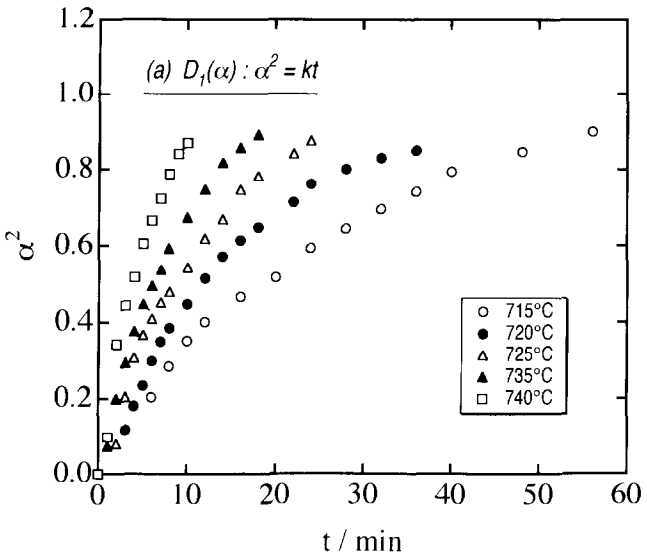

(a)

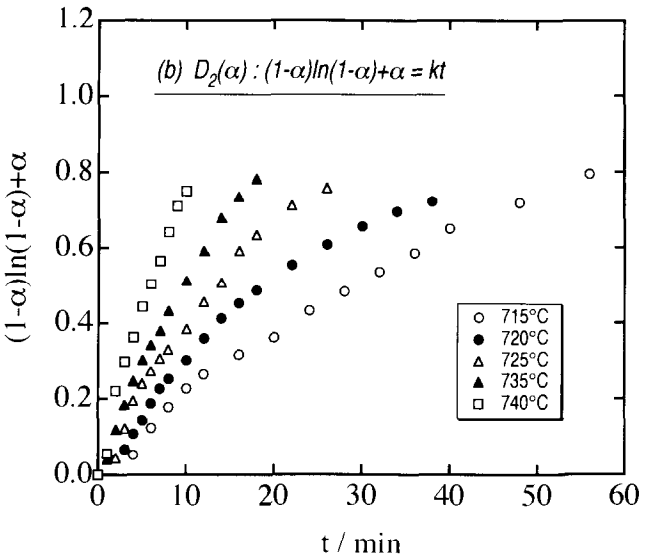

(b)

Fig. 4(a,b).

the partial oxygen pressure of the atmosphere P_{O_2} will strongly affect the rate of deoxygenation. Fig. 5 shows the XRD patterns of the products formed by pyrolysis under different values of P_{O_2} at 650°C for 1 h. With increasing P_{O_2} the intensity of the largest (112) peak of $LaCrO_3$ decreases, while the (120) peak of $LaCrO_4$ increases, indicating that the oxygen suppresses the deoxygenation of $LaCrO_4$.

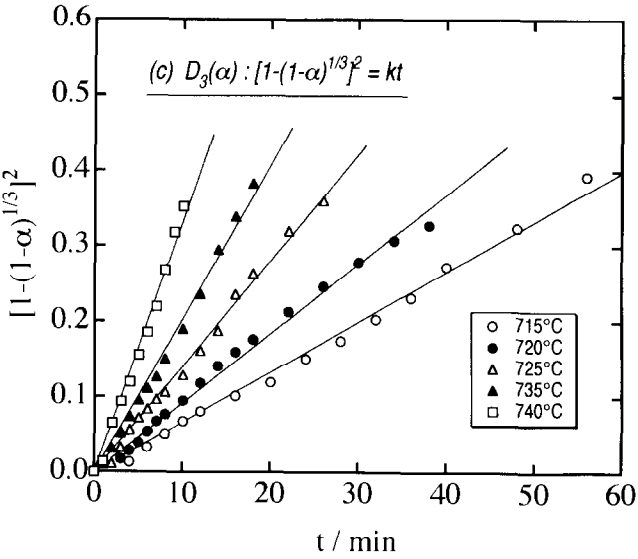

(c)

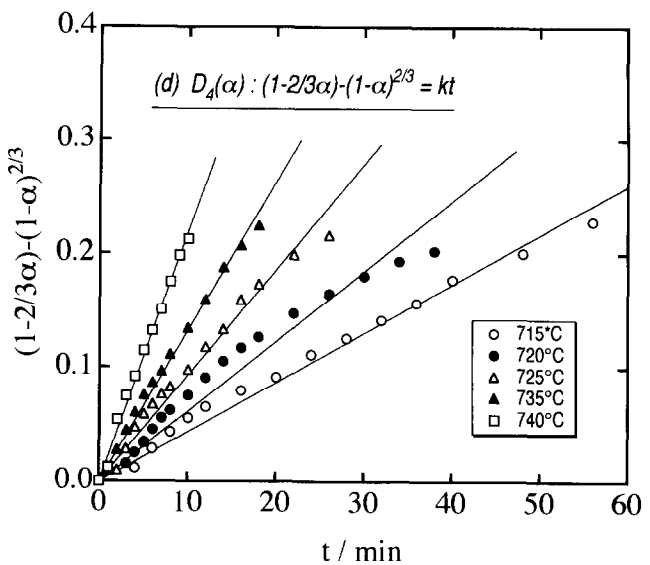

(d)

Fig. 4. Linear fittings of model functions for an O_2 atmosphere for data in Fig. 2(c): (a) $D_1(\alpha)$; (b) $D_2(\alpha)$; (c) $D_3(\alpha)$; (d) $D_4(\alpha)$.

Fig. 6 shows the morphologies of as-prepared $LaCrO_4$ and $LaCrO_3$ obtained after the isothermal TG measurements at 650°C in N_2. For $LaCrO_4$, some parallelogram-shaped crystals and many random shaped aggregates were observed on the macroscopic scale. They consist of spherical and ellipsoidal particles with diameters of 100–200 nm. The primary particles of $LaCrO_3$ also have similar

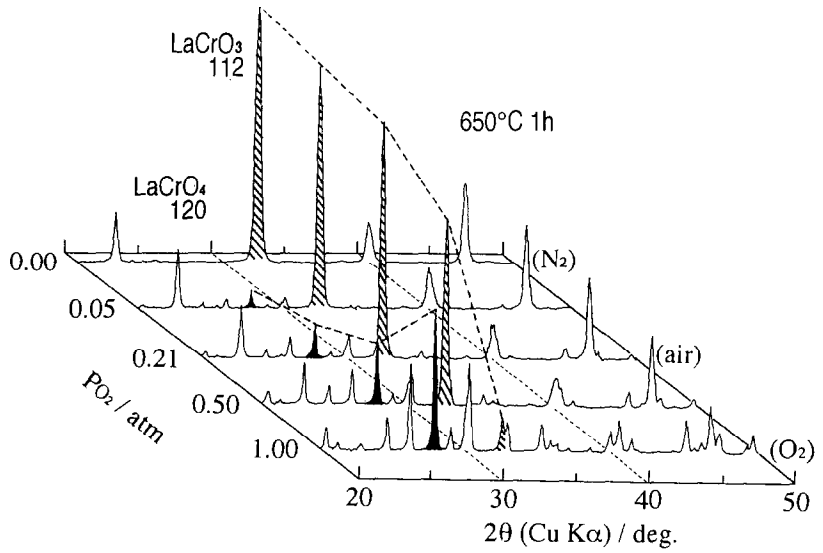

Fig. 5. XRD patterns of products formed by the pyrolysis of $LaCrO_4$ at 650°C for 1 h under different P_{O_2} values.

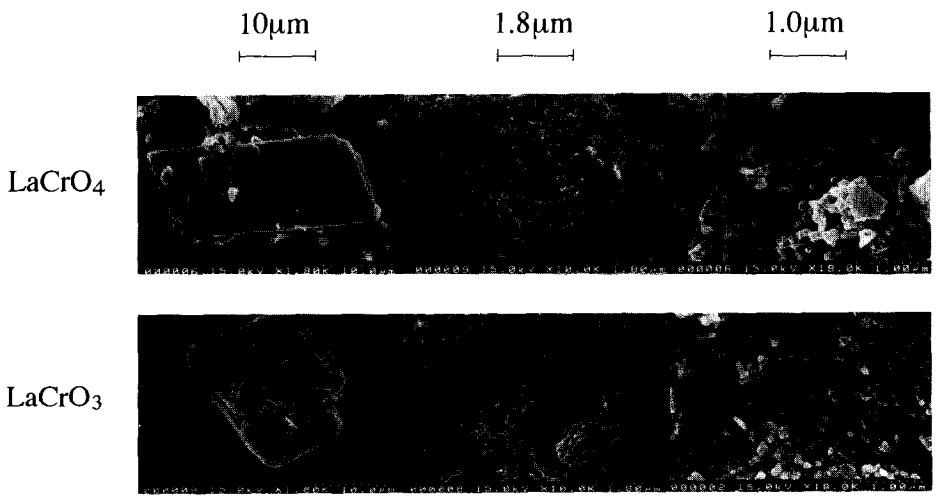

Fig. 6. SEM photographs of $LaCrO_4$ and $LaCrO_3$ powders. $LaCrO_4$ sample was as-prepared, and $LaCrO_3$ was formed after isothermal TG measurements at 650°C in N_2.

shapes and diameters to $LaCrO_4$. No cracks or gaps were observed on the surface of $LaCrO_3$ particles and they looked dense. The molecular volume and theoretical density of $LaCrO_4$ were 82.30 $Å^3$ molecule^{-1} and 5.15 g cm^{-3} respectively, and those of $LaCrO_3$ were 58.58 $Å^3$ molecule^{-1} and 6.77 g cm^{-3} respectively. Therefore, deoxygenation of $LaCrO_4$ causes about 30% decrease of molecular volume, but it

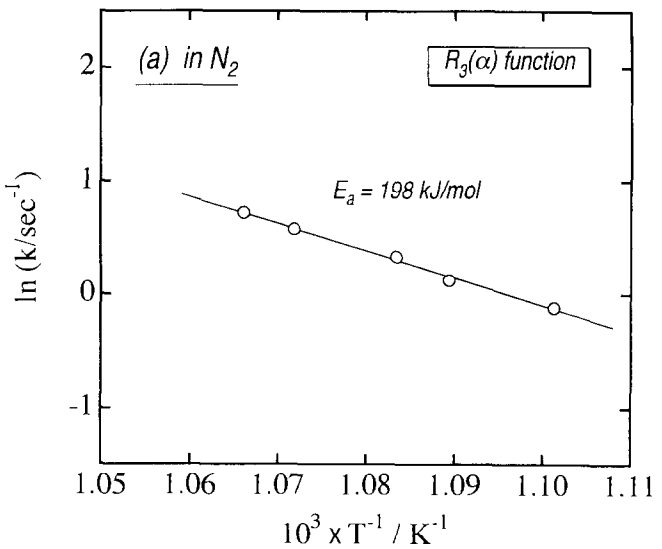

(a)

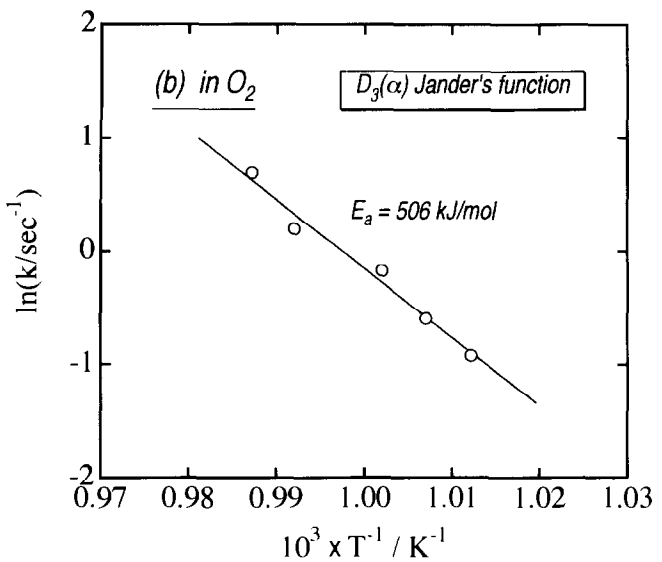

(b)

Fig. 7. Arrhenius plots of deoxygenation: (a) for $R_3(\alpha)$ function in N_2; (b) for the $D_3(\alpha)$ Jander function in O_2.

corresponds to only a 10% decrease in diameter in the case of spherical particles. It is likely that a marked contraction of the particles was not recognized in the SEM observation. These results suggest that the $D_3(\alpha)$ Jander model for deoxygenation kinetics cannot be rejected.

Rate constants at each temperature were determined from the slope of lines for the $R_3(\alpha)$ and $D_3(\alpha)$ Jander function. Fig. 7 shows the Arrhenius plots and

activation energies for the deoxygenations. The E_a value in O_2 (506 kJ mol^{-1}) is much larger than that in N_2. The value seems too large for a simple diffusion model, and it might suggest that the deoxygenation in O_2 proceeds via an intermediate state; for instance, oxygen species adsorbed on the $LaCrO_3$ surface prior to O_2 evolution.

Acknowledgments

We express our thanks to Mr Nodasaka and Dr Kodaira of Hokkaido University for the SEM and XRD analyses. A part of this work was carried out under the Visiting Researcher's Program of the Institute for Materials Research, Tohoku University, and by the Grant-in-Aid for Scientific Research (No. 04650637) from the Ministry of Education, Japan.

References

[1] C.P. Khattak and D.E. Cox, Mater. Res. Bull., 12 (1977) 463.
[2] S.C. Singhal, in International Materials Development for Solid Oxide Fuel Cells, DOE Report DOE/MC/21184, 1985.
[3] K. Kinoshita, F.R. McLarnon and E.J. Cairns, Fuel Cells Handbook, DOE/METC-88/6096, U.S. Department of Energy, Morgantown Energy Technology Center, Morgantown, WV, 1988.
[4] R. Koc, H.U. Anderson and S.A. Howard, in S.C. Singhal (Ed.), Proc. 1st Int. Conf. on Solid Oxide Fuel Cells, Florida, October, 1989, Electrochem. Soc., New Jersey, 1989, p. 220.
[5] H.U. Anderson, J.H. Kuo and D.M, Sparlin, in S.C. Singhal (Ed.), Proc. 1st Int. Conf. on Solid Oxide Fuel Cells, Florida, October, 1989, Electrochem. Soc., New Jersey, 1989, p. 111.
[6] R. Koc and H.U. Anderson, J. Mater. Sci. Lett., 11 (1992) 1191.
[7] R. Staut and P.E.D. Morgan, US Patent 3974108, 10 August 1976.
[8] A. Furusaki, H. Konno and R. Furuichi, Nippon Kagaku Kaishi, Part 6 (1992) 612.
[9] H. Schwarz, Z. Anorg. Allg. Chem., 322 (1963) 1.
[10] A. Roy and K. Nag, J. Inorg. Nucl. Chem., 40 (1978) 1501.
[11] S.G. Manca and E.J. Baran, J. Appl. Crystallogr., 15 (1982) 102.
[12] H. Konno, H. Tachikawa, A Furusaki and R. Furuichi, Anal. Sci., 8 (1992) 641.
[13] M. Nagayama, K. Goto and T. Tamura, Kinzoku Hyomen Gijyutsu, 19(7) (1968) 287.
[14] J.D. Hancock and J.H. Sharp, J. Am. Ceram. Soc., 55(2) (1972) 74.
[15] M. Avrami, J. Chem. Phys., 7(12) (1939) 1103; 8(2) (1940) 212; 9(2) (1941) 177.
[16] B.V. Erofe'ev, Dokl. Akad. Nauk. SSSR, 52 (1946) 511.
[17] W.A. Johnson and R.F. Mehl, Trans. AIME, 135(8) (1939) 416.